Instrument Science Report WFC3 2009-25

WFC3 SMOV Program 11427: UVIS Channel Shutter Shading

B. Hilbert
June 23, 2010

ABSTRACT

A series of internal flat field images and standard star observations were used to quantify the behavior of the UVIS channel shutter mechanism. Photometry of the stars and flat field analysis show that the UVIS shutter functionality in SMOV is comparable to that in ground testing. Shutter shading causes a variation in exposure time across the detector of no more than 0.0009 seconds. On-orbit ratios of actual versus commanded exposure times are also the same as in ground tests. The shutter fails to meet the repeatability requirement of 0.01 seconds, as expected from ground testing results (Hilbert, 2007). I also discuss additional photometric results.

Introduction

WFC3's UVIS channel shutter mechanism is identical to that of ACS. The shutter wheel is essentially a circle divided into four quadrants. Two of the quadrants are clear and two are closed. While the shutter motor is capable of moving the shutter wheel in either the clockwise or counter clockwise direction, the operations software limits the shutter motion to the clockwise direction only from the perspective of looking down the beam and onto the detector. In UVIS images, the shutter blade advances from the corner of amplifier D in the lower right corner, up to the corner of amplifier A in the upper left corner of the detector.

A 90° rotation changes the shutter from an open to closed position, or vice versa. For all commanded exposure times longer than 0.5 seconds, the shutter blade rotates out of the beam, stays in the open position for the commanded exposure time, and then rotates

in the same direction until the opposite shutter blade intercepts the beam, closing the shutter. For the minimum commanded exposure time of 0.5 seconds, the shutter does not stop its rotation during the exposure. (Baggett, 2002)

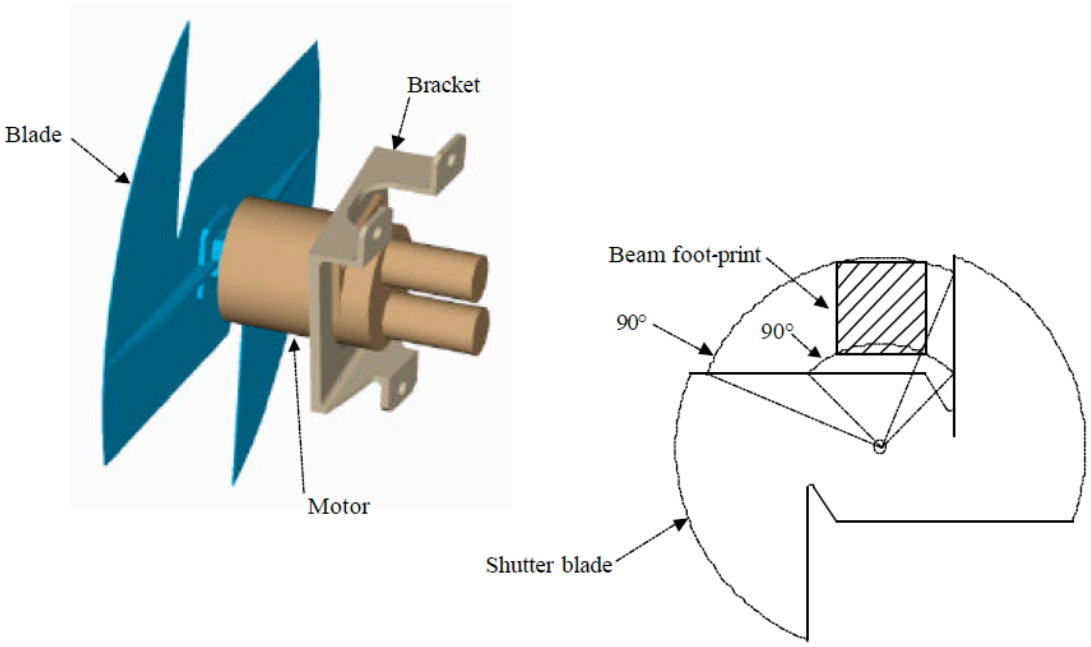

Figure 1: Graphical representation of the UVIS shutter mechanism, reproduced from the WFC3 OP-01 document (Baggett 2003).

This program's goals were to quantify shutter shading effects, as well as measure shutter timing and repeatability. If the shutter wheel were to move at a non-uniform velocity when opening or closing, the result would be a non-uniform exposure time across the detector, also known as shutter shading. A changing exposure time across the face of the detector would introduce a position dependence on photometry results.

The second effect we examined was the shutter accuracy. For a commanded exposure time, our goal was to measure the actual amount of time the detector was exposed to the beam.

Finally, we investigated the repeatability of the shutter. For a set of images commanded to have identical exposure times, we looked at the range of measured exposure times across the set.

These studies are a repeat of those done during the Thermal Vacuum 1 (TV1) and Thermal Vacuum 2 (TV2) ground testing campaigns.

Data

Observations

Observations were made in three separate Visits, the details of which are given in Table 6 in Appendex 1. During the first Visit, we collected 6 full-frame internal flat fields (illumination provided by the Tungsten lamp) with exposure times ranging from 0.5 seconds up to 17 seconds, to be used to search for shutter shading. Visits 2 and 3 each collected an identical set of observations of the standard star GD153 through the F395N filter. Exposure times varied from 0.5 to 30 seconds. F395N was chosen in order to avoid saturation in the longer exposures, but still achieve good signal-to-noise values of GD153 for the shorter of exposure times, enabling good measurements of shutter timing and repeatability.

In Visit 2 the target was placed in the B amp (upper right quadrant) of the UVIS detector and the UVIS1-C512B-SUB subarray was used, meaning only the B amp was read out. In Visit 3, the same exposures were taken, but with the target placed in the C amp (lower left quadrant) and the UVIS2-C512C-SUB subarray used, where only the C amp was read out. With the shutter traveling across the detector from the D towards the A amp, we chose to place GD153 in the B and C amps in order to minimize any differences in exposure time between the two due to shutter shading effects. In both cases, these subarrays resulted in images with dimensions of 512 x 513 pixels. All data associated with this prposal were collected in one block. In other words, HST did not perform any other observations between our Visits. However, our three Visits were not performed in order. Data for Visit 2 were collected first. This was followed by the flat field observations of Visit 1, and then by the standard star observations of Visit 3.

Exposure times for the set of images in Visits 2 ad 3 were arranged in random order, rather than monotonically increasing or decreasing to disentagle shutter shading effects in the short exposures from any variations in lamp brightness. During ground testing, we did not obtain information on the long-term stability of the illumination level but learned that we could more easily identify changes in the illumination level if the image exposure times were randomized. (Hilbert 2004)

Data Reduction

All files were reduced with version 1.4.1 of the CALWF3 pipeline. The reference files used are listed in Table 7 in Appendix 1. All reference files used were created from ground test data, except for an updated bias reference file created from on-orbit data.

The processing steps performed by CALWF3 depended on the type of data being reduced. The flat fields acquired in Visit 1 had the overscan pixel-derived bias level

subtracted, along with bias and dark current images subtracted. These steps, along with a flat field correction, we performed on the standard star observations in Visits 2 and 3.

After the initial processing by CALWF3, we used a separate tool to perform cosmic ray rejection on the GD153 images. We did not obtain images using CR-SPLITS, and option which is normally used to identify and remove cosmic rays by making a median image.

We therefore used the IRAF task L.A. Cosmic (van Dokkum, 2001) to identify and remove cosmic rays. See Table 8 in Appendix 1 for a list of parameters used in this procedure.

Analysis

Similar to analyses reported by Hilbert in past ISRs (WFC3 ISR 2004-14, WFC3 ISR 2007-17), we examined three aspects of shutter behavior. These included a search for shutter shading effects, a measure of the shutter accuracy relative to expectations, and a measure of the shutter repeatability. In the discussions below, we follow the standard lettering scheme for the 4 quadrants of the detector, shown in Figure 2. The amplifier A quadrant is the upper left quadrant of the detector. Amplifier B is the upper right quadrant. Amplifiers C and D are the lower left and right quadrants respectively. Table 1 shows photometry results for the mean image of each subarray/exposure time data set, using a 10 pixel radius aperture. Photometry results for all individual images are listed in Table 6 in the Appendix.

Visit	Array Size / Amp	Target	Exposure Time (sec)	Mean Measured Signal
1	Full Frame / ABCD	Tungsten Lamp	0.5	990 DN
			1.0	2083 DN
			17.0	35790 DN
2	512x512 / Amp B	GD153	0.5	3679 e^-
			0.7	5255 e^-
			0.8	6093 e^-
			1.0	7620 e^-
			30.0	229398 e^-
3	512x512 / Amp C	GD153	0.5	3733 e^-
			0.7	5366 e^-
			0.8	6229 e^-
			1.0	7743 e^-
			30.0	233253 e^-

Table 1: Photometry results for the mean image from each array size/exposure type. The units are DN for flat field images because gain is not applied during data reduction in CALWF3. However, gain is applied to the standard star observations, giving units of electrons. Gain values are listed in the CCDTAB file listed in Table 7, and are set to 1.53, 1.52, 1.56, and 1.55 e^-/DN for amps A, B, C and D respectively. Measured signal values for the flat field images are the sigma-clipped mean of each image, while those for the standard star observations are the results of the aperture photometry described in the text.

Shutter Shading

If the UVIS shutter rotates with a variable speed, pixels across the detector will experience a non-uniform exposure time. For example, if the shutter blade for a 0.5 second exposure were to begin rotating at a given speed and then slowly accelerate up to some terminal speed as it uncovered the detector, the area of the detector uncovered first will have a longer exposure time than the area uncovered last. If present, this effect would be visible as a large scale variation in brightness from the corner of the detector towards the center, as this is the direction of the shutter blade movement relative to the detector.

We searched for shutter shading in these SMOV data using the flat field images obtained in Visit 1. Because there are only 2 individual images for each exposure time, we created the mean image for that exposure time by calculating the simple mean at each pixel. We then took the ratio of the mean 17.0 second flat field image to the mean 0.5 second flat field image to remove any detector-dependent effects, such as spatial sensitivity differences. Any shutter shading effects, where the effective exposure time varies across the detector, will have a proportionally greater impact on the 0.5 second flat

compared to the 17.0 second flat, and will remain visible in the ratio image as changes in brightness across the detector.

The ratio image is shown in Figure 2. We see that quadrant 2 (lower left) seems to have a higher mean value compared to the other four quadrants. Using IDL's resistant_mean.pro procedure, we calculated the mean value in each of the four quadrants, along with the difference from the expected value of 34 (= 17 sec/0.5 sec). The results are shown in Table 2.

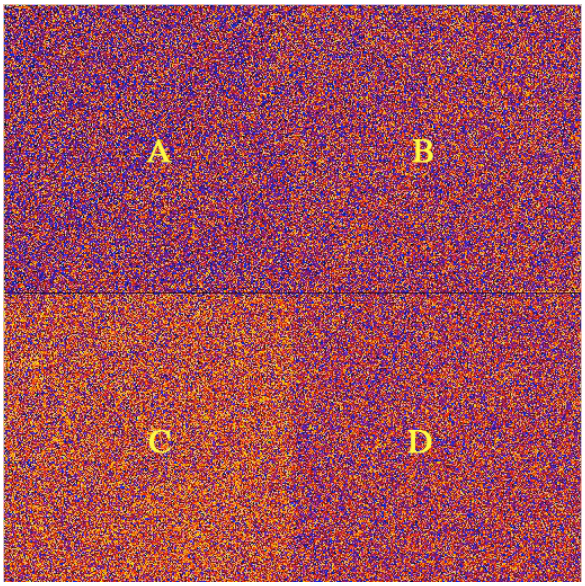

Figure 2: Ratio image of the mean 17.0 second flat to the mean 0.5 second flat, with the amplifier corresponding to each quadrant labeled. This is a histogram equalization stretch, ranging from 34 to 38.4. In this color scheme, blue represents the lowest values, with red, orange, and yellow representing successively higher values.

	Amp A	**Amp B**	**Amp C**	**Amp D**
Mean Signal Ratio	36.028	36.109	36.313	36.149
Robust Standard Deviation	0.71	0.68	0.68	0.64
% From Expected	5.96	6.20	6.80	6.32

Table 2: Mean values for the 17-second over 0.5 second flat field ratio. All 4 quadrants show a ratio value above the expected value of 34. The bottom row can be interpreted as both the percentage above the expected ratio value, as well as the percentage of signal deficit in the 0.5 second image compared to expected. Mean values and errors calculated from IDL's resistant_mean.pro and robust_sigma.pro.

The quadrant-to-quadrant differences shown above appear similar to those seen in Thermal Vacuum 2 (TV2) testing (Hilbert 2007). The fact that the mean ratio values are above the expected value of 34 implies that either the 0.5 second flat fields measured less

flux than expected, or the 17 second flats measured more than expected. The shutter accuracy portion of this analysis addresses this issue more directly, and will present the relevent results.

In order to search more effectively for shutter shading artifacts in the ratio image, we added offsets to the four quadrants in order to remove the mean signal differences seen in Figure 2 and Table 2. In order to do this, we averaged together 1650 rows from amps A and B to create a single mean row. We then repeated this process for amps C and D. Figure 3 shows a plot of the signal in the mean rows. We calculated the mean value in the 100 pixels on the amp A side nearest to the amp A/amp B boundary, as well as the 100 pixels on the amp B side nearest the boundary. We added the difference between these two means to all pixels in amp A, bringing them up to amp B's mean signal level. The process was then repeated between amp C and amp D, bringing amp C down to amp D's mean signal level.

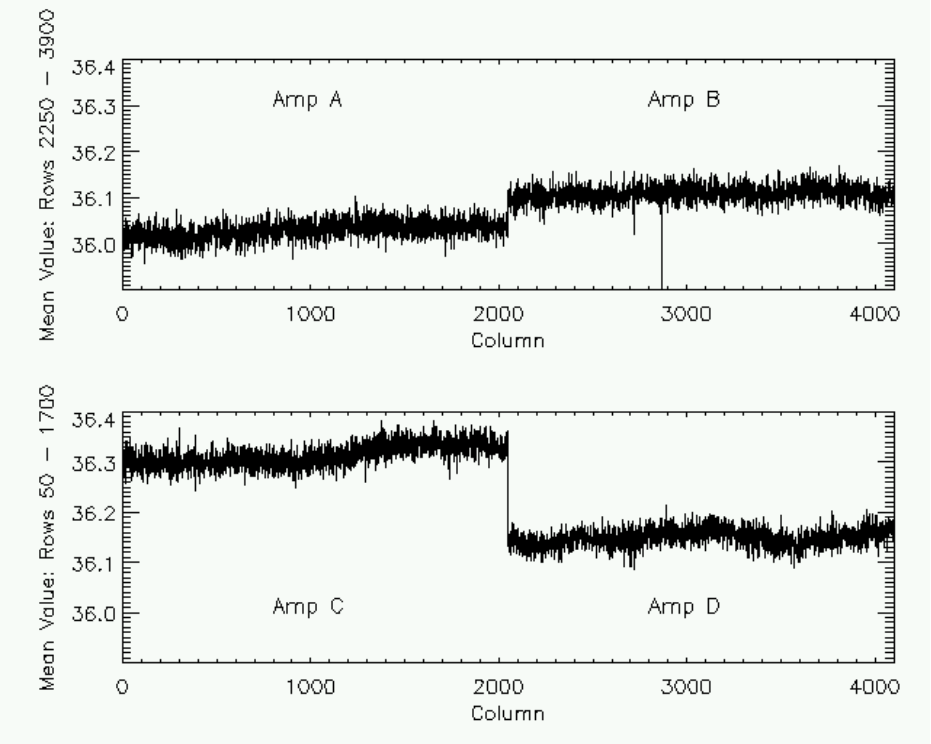

Figure 3: Plot of the signal in the ratio image along two mean rows. Each row was created by calculating the resistant mean across 1650 rows.

We then brought the mean signal level of the amp C/amp D chip to match that of the amp A/amp B chip through a similar process. In this case we created a mean column from 1000 columns across amps B and D, calculated the mean value on each side of the amp boundary, and added the difference to all pixels in amps C and D. Figure 4 shows the ratio image after these adjustments were completed. The differences in mean signal between the four quadrants are no longer visible.

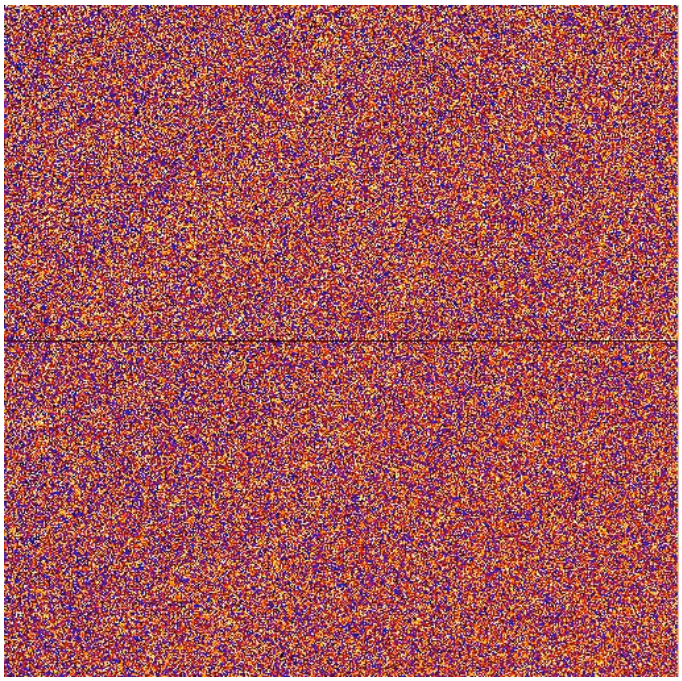

Figure 4: Long flat over short flat ratio image after the mean signal offsets were removed.

Finally, we manually inserted 31 rows of pixels between chip 1 and chip 2 in order to mimic the inter-chip gap of the detector. (Platais, priv. comm.) This provided the most realistic detector geometry over which the shutter blade passed while taking data.

Once these steps were complete, we began our search for shutter shading effects. Similar to the analysis performed on the ground testing data, we attempted to quanitfy any shutter shading effects by fitting a surface to the ratio image presented in Figure 4. Since we have no knowledge of the shutter mechanism's exact velocity profile during operation, we have no reason to assume one shutter shading morphology over another.

As with the ground testing data, we fit both a plane and a quadrantic surface to the ratio image, and examined the residuals in both cases to determine the best shutter shading model, and to quantify the variation in signal and exposure time. We find that the planar surface is a better fit to the data than the quadratic surface, with a variation in exposure time across the detector roughly an order of magnitude less than the CEI Specification (4.5.2) of 0.01 seconds. From this point on, we will discuss only the planar surface fit results. Table 3 gives the results of the surface fitting, including the variation in effective exposure time across the chip.

As a check on effects of our added mean level offsets to the various quadrants, we also performed the surface fitting to the original uncorrected ratio, seen in Figure 2. These results are also presented in Table 3. Even in the case of the uncorrected signal offsets, we find that the effective exposure time variation across the detector is still less than the CEI Specification. However, removing the signal offsets between the quadrants should allow for better fitting to any true shutter shading effects.

	% Variation Across Detector	Exposure Time Variation Across Detector (sec)	Mean of Residuals (DN)	Standard Deviation of Residuals (DN)
Signal Offsets Removed	0.18%	0.0009	-0.0031	0.6739
Uncorrected Signals	1.57%	0.0078	-0.0063	0.6819

Table 3: Shutter shading surface fitting results. The top row gives results for the raio image after the mean signal level differences between quadrants was removed. The bottom row shows the results of the surface fitting on the uncorrected ratio image. The variations listed in the first column are percentages relative to the minimum signal in the fitted surface. Residuals in columns 3 and 4 are for the difference between the ratio image and the fitted surfaces.

Figure 5 shows the best-fit planar surface, which agrees well with the shutter geometry. The high ratio value in the amp D corner decreases slowly in the direction of shutter travel, toward the amp A corner. Since the ratio image is of the long exposure flat field over the short exposure flat field, and we work under the assumption that any shutter shading effects will have a larger effect in shorter exposure times, the higher ratio values in the corner of amp D indicate lower effective exposure times there in the 0.5 second flat field image. As indicated in the top row of Table 3, the planar fit shown in Figure 5 reveals a 0.0009 second difference in exposure time betwen the amp A and amp D corners. From this, we can say that the UVIS channel meets the CEI Specification for shutter shading.

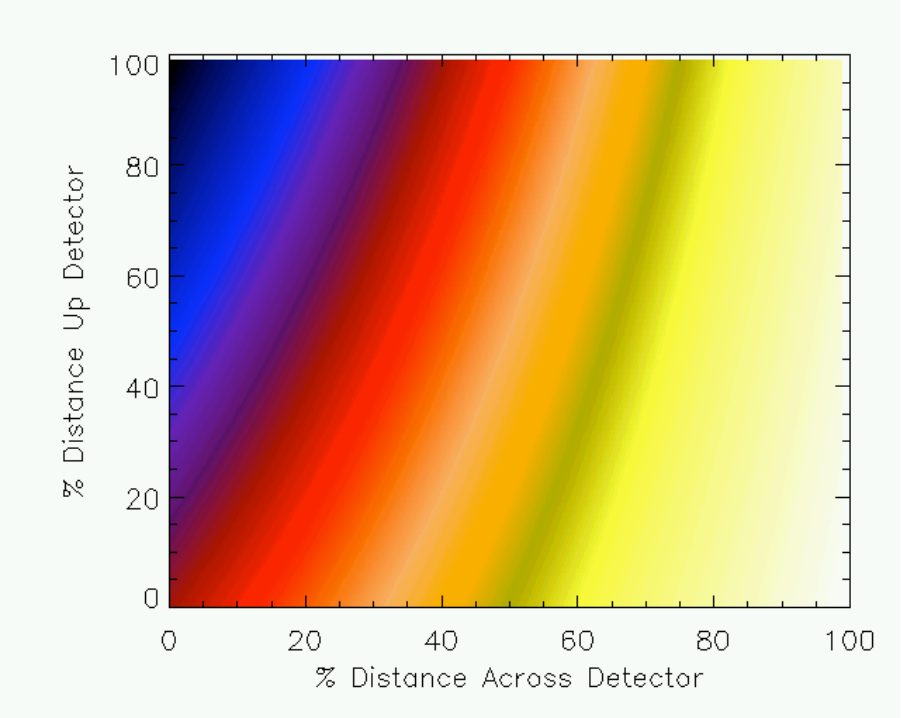

Figure 5: Contour plot of the fitted plane to the ratio image shown in Figure 4. The ratio values range from 36.062 in the upper left corner (amp A) to 36.125 in the lower right corner (amp D), in a direction slightly more horizontal than the detector diagonal. This implies a longer effective exposure time for the amp A corner relative to the amp D corner.

Shutter Accuracy

Although there is no formal CEI Specification for shutter accuracy, we still wished to compare the actual exposure times of images versus their commanded exposure times. We accomplished this by using commanded exposure times, and comparing the measured count rates for long versus short exposure images. In the ideal case where the UVIS shutter was open for exactly the commanded exposure time in both cases, this countrate ratio would be equal to 1.0. Values less than 1.0 imply that the shutter was open for less than the commanded exposure time in the image with the shorter nominal exposure time. For the purposes of this analysis, we assume that any deviation from a countrate ratio of 1.0 is due to an exposure time difference in the shorter image. In other words, we assume that any difference between the actual and commanded exposure time in the long images is a small source of error compared to differences in the images with shorter exposure times. For example, an error of 0.1 seconds in a 30 second image represents only a 0.33% error, while the same difference in exposure time represents a 20% error on a nominal 0.5 second image.

Slightly different methods were used in performing these calculations on the flat field observations versus the standard star observations due to the differences in the distribution of high signal pixels. In the case of the flat field observations, we used the mean images described in the shutter shading section above. By dividing each mean image by its commanded exposure time, we created a mean countrate image. We then divided the mean 0.5-second and 1.0-second countrate images by the mean 17-second countrate image. Using IDL's resistant_mean.pro and robustsigma.pro, we then calculated the mean and standard deviation of the countrate ratio. Results are presented in Table 4 and discussed below.

The method used for the standard star observations was slightly different, due to the fact that the only high signal area on the chip was the point source. Similar to what was done initially for the shutter shading examination, we first created a mean image corresponding to each amplifier/exposure time combination in Table 4. In this case, we had either 11 images (for exposure times less than 1.0 seconds) or 6 images (for exposure times of 1 second or more) of each exposure type. We therefore used IDL's resistant_mean.pro script on a pixel-by-pixel basis to produce a sigma-clipped mean image for each exposure time/amplifier combination.

We performed aperture photometry on these mean images. In order to avoid any variations in the PSF from effects such as telescope breathing, we used an aperture with a radius of 10 pixels to enclose the source in each image. Background signal in each image was calculated in an annulus with an inner radius of 40 pixels and an outer radius of 100 pixels. The photometry result for each image was then divided by the commanded exposure time for that image, in order to produce a measure of the target's countrate for that image. Finally, the countrates were all divided by the countrate measured in the mean 30 second image.

Table 4 gives the countrate ratio results for all data in this proposal, as well as results from TV1 and TV2 testing as a reference. Uncertainties are derived using IDL's robust_sigma.pro in the case of the flat field ratio images, and are the formal errors on the photometry propagated into the countrate ratios in the case of the GD153 observations.

We find differences when comparing the shutter accuracy results from the GD153 observations to those derived from the flat field observations. Specifically, for a given exposure time, the shutter timing results using the point source observations show higher countrate ratios and therefore exposure times closer to expectations compared to the results derived from flat fields.

Figure 6 is a graphical representation of the data presented in Table 4. From this we see that the flat field observations (blue points) are farther from the commanded exposure time compared to the point source observations (red points), but are consistent within the

uncertainties. Differences between the amp B and amp C observations are well within the calculated uncertainties and imply no difference in exposure time between the two quadrants of the detector.

In the case of the 0.5 second flat field exposures, we see that the countrate ratios of 94% – 96% are consistent with the measured signal ratio values above the expected value of 34 in Table 2 for the shutter shading results.

Commanded Exposure Time (sec)	Amp	Countrate Ratio	Robust Standard Deviation of Ratio	Calculated Exposure Time (sec)	Countrate Ratio in TV1 / TV2 (all flat fields)
0.5	All	0.941	0.018	0.470	0.990 / 0.944
1.0	All	0.990	0.013	0.990	0.990 / 0.990
0.5	B	0.962	0.017	0.481	0.990 / 0.944
0.5	C	0.960	0.017	0.480	0.990 / 0.944
0.7	B	0.982	0.014	0.687	0.981 / 0.986
0.7	C	0.986	0.014	0.690	0.981 / 0.986
0.8	B	0.996	0.013	0.797	0.991 / 0.995
0.8	C	1.002	0.013	0.802	0.991 / 0.995
1.0	B	0.996	0.012	0.996	0.990 / 0.990
1.0	C	0.996	0.012	0.996	0.990 / 0.990

Table 4: Countrate ratios of the mean images from internal and external observations. Internal observations, taken with the Tungsten lamp in Visit 1, are in the top two rows. The remaining rows are for observations of GD153.

Shutter accuracy observations taken in TV1 and TV2 were full-frame flat fields. (Hilbert 2007) Comparing the SMOV flat field results (shaded rows of Table 4) to those from ground testing, we see very similar results, with the exception of the 0.5 second data from TV1. In TV2 testing the countrate ratios were calculated to be 0.944 and 0.990 for the 0.5 and 1.0 second flats respectively, compared to the SMOV values of 0.941 and 0.990. Standard deviations of the ratios obtained with TV1 and TV2 datasets were not published. We therefore assume similar uncertainties to those calculated here.

Under this assumption, our SMOV-derived countrate ratios are also consistent with TV1 and TV2 values in the case of the 0.7 and 0.8 second data, despite the fact that this is comparing flat field data from ground testing with point source data from on-orbit. In the case of 0.7 second exposures, the countrate ratios measured in TV1 and TV2 were 0.981

and 0.986, compared to our values of 0.982 and 0.986. From these results we can say that the UVIS shutter has been consistent in its behavior from TV1 up through SMOV.

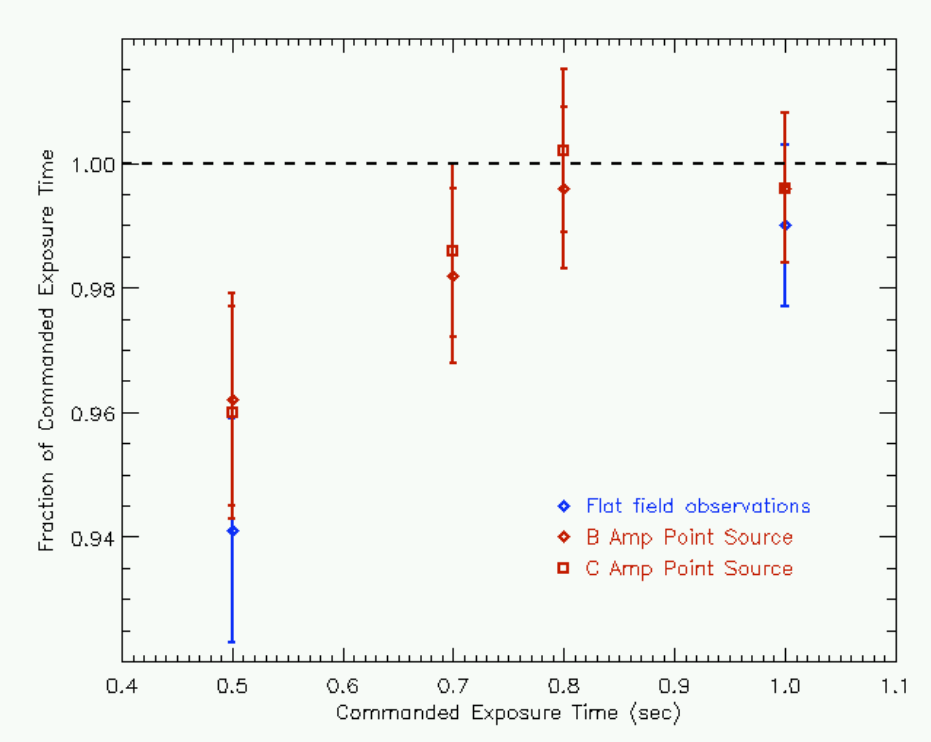

Figure 6: Shutter accuracy results derived from photometry on the mean image for each commanded exposure time presented in Table 4.

Shutter Repeatability

To determine the repeatability of the shutter, we performed aperture photometry on images of GD153 taken using both the B and C amps, and used those results to measure exposure times. Our goal was to compare the exposure time variation across a set of observations with a single commanded expoure time. The CEI Specification (4.5.2) states that for a set of images with a single commanded exposure time, the measured exposure times cannot vary by more than 0.01 seconds across the set.

This test has fallen victim to small number statistics in the past. During TV2 testing, we obtained 16 images at most for a given exposure time. In some cases, there were as few as 4 images. (Hilbert 2007) The situation in the SMOV test are similar. For times less than 1.0 second, we have 11 images at each exposure time. For 1.0 and 30.0 second exposure times, we have only 6 images each.

Similar to the method used in the shutter accuracy analysis, we began by using aperture photometry to calculate the total signal from GD153 on each image from Visits

2 and 3. As with the mean images in the previous section, we used an aperture with a 10 pixel radius to measure the source flux, and calculated the background level in an annulus with an inner radius of 40 pixels and an outer radius of 100 pixels. Photometry results for each image are presented in Table 6 in the Appendix. We then divided each image's signal by its commanded exposure time, in order to produce a measured countrate for each image.

Figure 7 shows the results of the photometry, translated into countrates through division by commanded exposure time. Each panel in Figure 7 shows the measured signal rate for a different commanded exposure time. Similar to what is seen in Figure 6 and the shutter shading analysis, the images with shorter exposure times show a lower measured signal rate when compared to the longer exposures. In this figure, we also distinguish between images taken with the "A" shutter blade (blue points) versus those with the "B" shutter blade (red points). The specific shutter blade used for each observation was determined by examining the ISHRBPOS keyword in the second extension header in the spt file associated with each image. This keyword returns a step value corresponding to the position of the shutter wheel. The step values can range from 0 to 65536, which cover 2 full rotations of the shutter wheel. An image is then defined as using a particular shutter blade according to the following rules. If ISHRBPOS is between 800 and 2100, or between 33600 and 34900, then the shutter blade used is the "B" blade. If ISHRBPOS is between 17200 and 18500 or between 50000 and 51300, then the image uses the "A" blade. (Howard Bushouse, priv. comm.) Keyword values outside of these ranges represent positions where a shutter blade is partially covering the detector, and should not be present in the image headers.

In TV2 testing, there was a clear correlation between the measured signal level and the shutter blade for the 0.5-second images, (see Figure 3 in Hilbert 2007) where the "B" blade consistently exhibited a measured exposure time closer to the commanded exposure time compared to the "A" blade. In Figure 7, blue points represent images taken with the "A" shutter blade, while red points are for those that used the "B" blade. In the panel containing the 0.5 second data results, there does not appear to be any obvious corellation between shutter blade and measured signal rate.

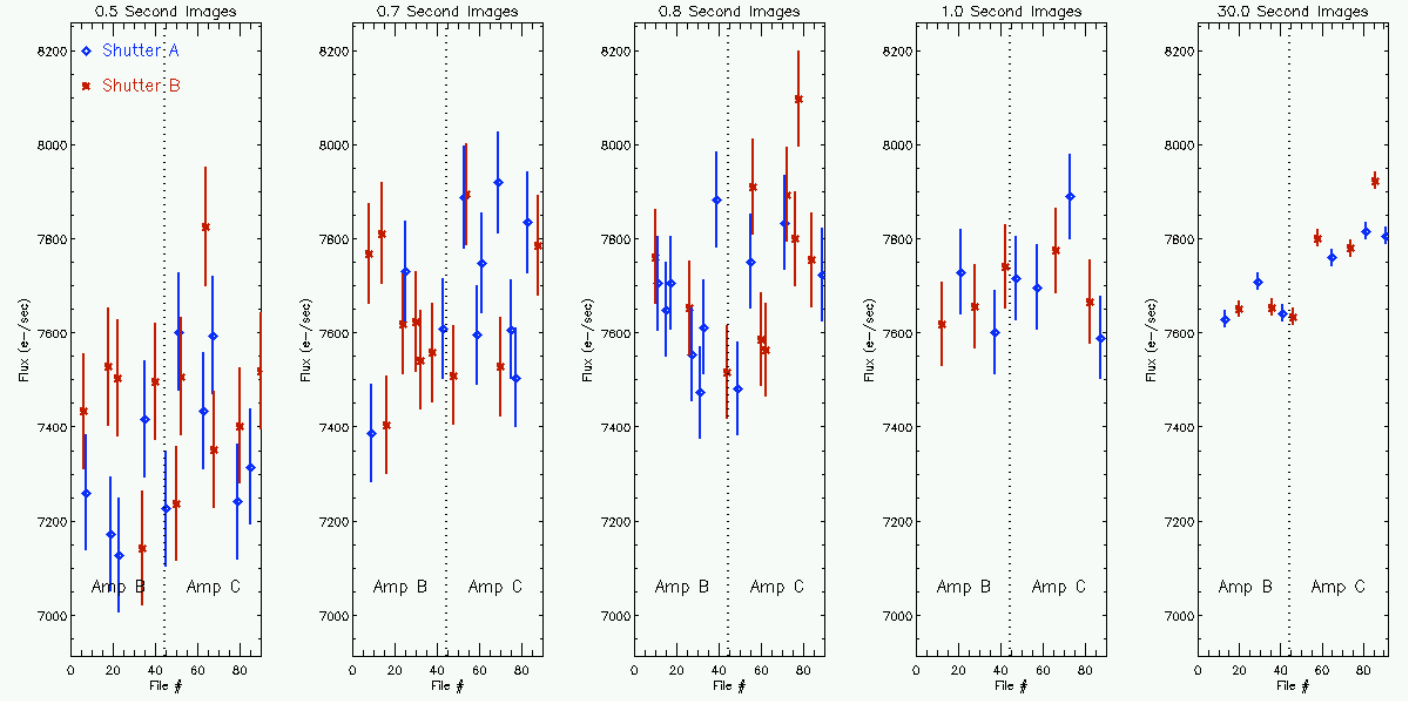

Figure 7: Measured countrates from each of the individual observations of GD153. Error bars are formal (Poisson) photometry error divided by commanded exposure time.

Unlike in the shutter accuracy portion of the analysis, we deal here with individual images, rather than mean images. This allows us the opportunity to examine the measured effective exposure times of the individual 30 second images, which were averaged into the denominator of the ratio image during shutter accuracy analysis and therefore unable to be analyzed separately. The large signal to noise ratio in the 30 second images reduces the error bars on the photometry results enough to unambiguously show a difference in the photometry results between amps B and C which were only suggested by the images with shorter exposure times.

The right-most panel in Figure 7 shows that images with the point source located in amp B exhibited systemitically less flux than when the point source was in amp C. This is reminiscent of the mean signal offsets seen in the shutter shading flat field analysis (Figure 2), although the effect here is greater in magnitude, with amp B sources showing ~2% less flux than those in amp C. There are hints of similar results in the 0.7 and 0.8 second data, although it is difficult to make any definitive claims given the large uncertainties on these data. Possible sources of this difference in source brightness include errors in the ground testing-derived UVIS flat field and overscan subtraction errors.

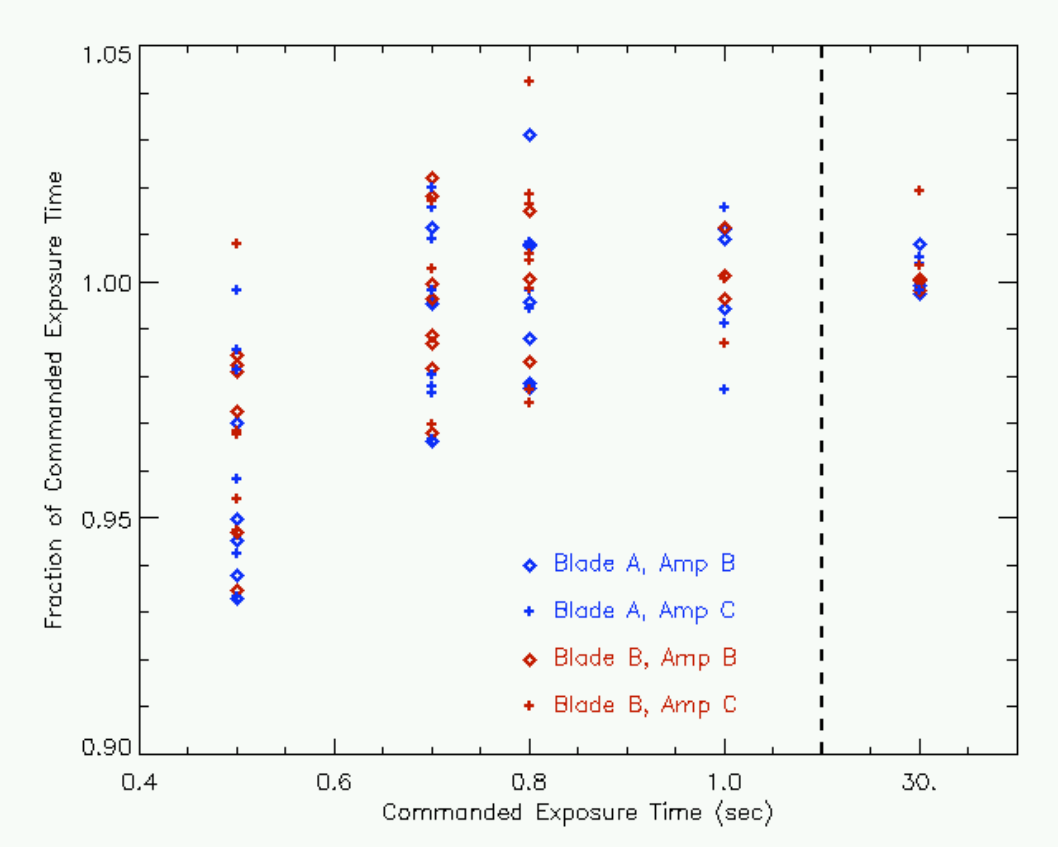

Figure 8: Countrate ratios calculated for each of the individual images of GD153, with distinctions made for each of the two shutter blades as well as the amplifier used.

Finally, we divided the countrate values in Figure 7 by that calcuated for the mean 30 second image. This produced countrate ratio values similar to those seen in the shutter accuracy testing in Figure 6. Figure 8 shows the countrate ratio values for all data in Visits 2 and 3.

Multiplying the countrate ratios in Figure 8 by the commanded exposure times, we calculated actual exposure times for all images. Table 5 shows details of these measured exposure times for each amplifier/exposure time dataset. The third column lists the sigma-clipped mean measured exposure time for each dataset. These values differ from those in the 5th column of Table 4. This is due to the fact that the calculated exposure times in Table 4 are the result of photometry performed on mean images, whereas the values in Table 5 are means of photometry performed on individual images. Despite the differences, the values are consistent within the stated uncertainties.

The fourth column of Table 5 shows the robust standard deviation of the exposure times in each dataset, as a percentage of the mean exposure time. These uncertainties include contributions from a number of sources in addition to the actual variation in exposure time. With the high signal levels, the contribution of read noise to these uncertainties is negligible, but Poisson noise from the sources is significant. Using the signal levels listed in Table 1, we subtracted the Poisson noise in quadrature from the

uncertainties listed in column 4. This resulted in the uncertainties listed in column 5, which more closely represent the true variation in exposure time for each data set. In column 6, we convert these percentages back into units of seconds, to arrive at the RMS variation in exposure time for each commanded exposure time. Note that with the limited number of images for each exposure time, small number statistics do have an effect. For the 1.0-second images taken with shutter blade B, we see variations in exposure time less than Poisson statistics suggest we should, even if the shutter were perfectly repeatable. This is due to there being only 6 images for this particular part of the analysis.

Commanded Exposure Time (sec)	Amp	Sigma-Clipped Mean Measured Exposure Time (sec)	Stdev as Percentage of Mean Exposure Time	Remove Poisson Noise	RMS Variation in Exposure Time (sec)	Number of Images in Dataset
0.5	B	0.479	2.51%	1.89%	0.0095	11
0.5	C	0.482	2.49%	1.88%	0.0094	11
0.7	B	0.695	1.87%	1.26%	0.0088	11
0.7	C	0.695	2.16%	1.67%	0.0117	11
0.8	B	0.799	1.75%	1.19%	0.0095	11
0.8	C	0.802	2.00%	1.55%	0.0124	11
1.0	B	1.004	0.80%	ERR	ERR	6
1.0	C	0.994	1.51%	0.99%	0.0099	6
30.0	B	29.973	0.26%	0.15%	0.0450	6
30.0	C	30.066	0.53%	0.49%	0.1470	6

Table 5: Shutter repeatability results. The third column lists the sigma-clipped mean measured exposure time for each type of exposure. The fourth column lists the robust standard deviation in exposure time as a percentage of the mean exposure time. The fifth column lists the variation after removing the contribution from Poisson noise on the signal, and the sixth column translates the percentage variations into temporal variations. The CEI Specification that we are comparing to states that images should not vary in exposure time by more than 0.01 seconds.

Conclusions

From the data obtained in HST proposal 11427, we find the following results concerning the UVIS channel's shutter behavior:

Based on internal flat field data, we find from shutter shading analysis that the exposure time across an image varies by 0.0009 seconds. This is an order of magnitude

better than the CEI Specification of 0.01 seconds. Based on this, we find that no shutter shading correction is necessary in the CALWF3 data reduction pipeline.

Comparisons of measured exposure times versus commanded exposure times indicate that the on orbit UVIS shutter performance is consistent with that in ground tests. For a commanded exposure time of 0.5 seconds, the results indicate that the shutter is actually open 3.8 – 4.0% less (0.480 – 0.481 seconds). For images with a commanded exposure time of 0.7 seconds, the measured exposure times were 0.687 – 0.690 seconds. For all other exposure times, the calculated exposure times were consistent with the commanded exposure times to within the measurement uncertainty.

The shutter mechanism appears to meet the CEI Specification for shutter repeatability for most short exposure times. For commanded exposure times of 1.0 second and less, the standard deviation of the measured exposure times in a set of identical images is up to 0.0124 seconds. This may be partially the fault of the low signal levels associated with the short exposures and the small number of exposures collected at each exposure time. In order to avoid saturating the longest exposures, we were forced to use a narrow band filter, which severely limited the number of counts in the short exposures.

Unresolved Issues

The cause behind the amp to-amp mean signal level offset shown in Figure 2 is still unknown. Fortunately this is a small effect (0.8% between the highest and lowest amps), but the cause is mostly likely in the initial data reduction steps, and should be tracked down.

Possibly related to this is the observed amplifier dependent photometry results shown in Figure 7. The direction of offset between the B and C amps is consistent with the mean offset level described above, but of a larger magnitude. As shown in the 30-second images in Figure 7, the photometry results for the amplifier B images reveal roughly 2% lower flux levels than those using amplifier C.

STScI currently makes no correction to users' data to correct for the difference between commanded and actual exposure time for short exposures. This correction would only be significant for 0.5 and 0.7-second images. A proposed fix is in progress, where the EXPTIME header keyword for 0.5 and 0.7-second exposures will be changed from the commanded exposure time to values in line with the results found here.

Acknowledgements

Thanks to Tiffany Borders and Sylvia Bagget for providing an updated bias image from on-orbit data.

References

Baggett, W. 2003. **Operations and Data Management Plan for the Wide Field Camera 3 (WFC3)**. CDRL No. OP-01. http://www.stsci.edu/instruments/wfc3/WOWG/wfc3-op01-draft.pdf

Hilbert, B. 2004. "***Stability and Accuracy of the UVIS Shutter"***. WFC3 ISR 2004-14, December 2004.

Hilbert, B. 2007. ***"WFC3 TV2 Testing: UVIS Shutter Stability and Accuracy"***. WFC3 ISR 2007-17. August 2007.

van Dokkum, 2001. PASP, 113, 1420 (info at http://www.astro.yale.edu/dokkum/lacosmic/)

Hubble Space Telescope Wide Field Camera 3 Contract End Item Specification. Hubble Space Telescope Library #TM-027550. May 2000.

Appendix 1

Table 6: List of observations associated with SMOV proposal 11427. All three Visits were performed consecutively, although not in order. Data for Visit 2 were collected first, followed by Visit 1 and finally, Visit 3. The aperture photometry results presented in the right-most column are for an aperture with a radius of 10 pixels. For the flat field observations, the photometry results are the sigma-clipped mean signal per pixel.

Visit	Filename	Aperture Used	Exposure Time (sec)	Target	Counts (e^-)
1	iaai01rqq	UVIS (Full Frame)	0.5	TUNGSTEN	956
1	iaai01rrq	UVIS (Full Frame)	0.5	TUNGSTEN	980
1	iaai01rtq	UVIS (Full Frame)	1	TUNGSTEN	2040
1	iaai01ruq	UVIS (Full Frame)	1	TUNGSTEN	2034
1	iaai01rwq	UVIS (Full Frame)	17	TUNGSTEN	35131
1	iaai01rxq	UVIS (Full Frame)	17	TUNGSTEN	35135
2	iaai02qgq	UVIS1-C512B-SUB (AMP B)	0.5	GD153	3716.2
2	iaai02qhq	UVIS1-C512B-SUB (AMP B)	0.5	GD153	3629.8
2	iaai02qiq	UVIS1-C512B-SUB (AMP B)	0.7	GD153	5437.5
2	iaai02qjq	UVIS1-C512B-SUB (AMP B)	0.7	GD153	5170.6
2	iaai02qkq	UVIS1-C512B-SUB (AMP B)	0.8	GD153	6208.2
2	iaai02qlq	UVIS1-C512B-SUB (AMP B)	0.8	GD153	6163.5
2	iaai02qmq	UVIS1-C512B-SUB (AMP B)	1	GD153	7618.3
2	iaai02qnq	UVIS1-C512B-SUB (AMP B)	30	GD153	228857

2	iaai02qoq	UVIS1-C512B-SUB (AMP B)	0.7	GD153	5467.7
2	iaai02qpq	UVIS1-C512B-SUB (AMP B)	0.8	GD153	6118.9
2	iaai02qqq	UVIS1-C512B-SUB (AMP B)	0.7	GD153	5182.8
2	iaai02qrq	UVIS1-C512B-SUB (AMP B)	0.8	GD153	6164.0
2	iaai02qsq	UVIS1-C512B-SUB (AMP B)	0.5	GD153	3763.5
2	iaai02qtq	UVIS1-C512B-SUB (AMP B)	0.5	GD153	3585.8
2	iaai02quq	UVIS1-C512B-SUB (AMP B)	30	GD153	229513
2	iaai02qvq	UVIS1-C512B-SUB (AMP B)	1	GD153	7728.7
2	iaai02qwq	UVIS1-C512B-SUB (AMP B)	0.5	GD153	3751.7
2	iaai02qxq	UVIS1-C512B-SUB (AMP B)	0.5	GD153	3563.2
2	iaai02qyq	UVIS1-C512B-SUB (AMP B)	0.7	GD153	5332.3
2	iaai02qzq	UVIS1-C512B-SUB (AMP B)	0.7	GD153	5411.3
2	iaai02r0q	UVIS1-C512B-SUB (AMP B)	0.8	GD153	6121.5
2	iaai02r1q	UVIS1-C512B-SUB (AMP B)	0.8	GD153	6041.9
2	iaai02r2q	UVIS1-C512B-SUB (AMP B)	1	GD153	7655.7
2	iaai02r3q	UVIS1-C512B-SUB (AMP B)	30	GD153	23127
2	iaai02r4q	UVIS1-C512B-SUB (AMP B)	0.7	GD153	5336.2
2	iaai02r5q	UVIS1-C512B-SUB (AMP B)	0.8	GD153	5978.2
2	iaai02r6q	UVIS1-C512B-SUB (AMP B)	0.7	GD153	5278.9
2	iaai02r7q	UVIS1-C512B-SUB (AMP B)	0.8	GD153	6089.4
2	iaai02r8q	UVIS1-C512B-SUB (AMP B)	0.5	GD153	3571.1
2	iaai02r9q	UVIS1-C512B-SUB (AMP B)	0.5	GD153	3708.4
2	iaai02raq	UVIS1-C512B-SUB (AMP B)	30	GD153	229605
2	iaai02rbq	UVIS1-C512B-SUB (AMP B)	1	GD153	7600.7
2	iaai02rcq	UVIS1-C512B-SUB (AMP B)	0.7	GD153	5290.3
2	iaai02rdq	UVIS1-C512B-SUB (AMP B)	0.8	GD153	6305.4
2	iaai02req	UVIS1-C512B-SUB (AMP B)	0.5	GD153	3748.1
2	iaai02rfq	UVIS1-C512B-SUB (AMP B)	30	GD153	229232
2	iaai02rgq	UVIS1-C512B-SUB (AMP B)	1	GD153	7739.8
2	iaai02rhq	UVIS1-C512B-SUB (AMP B)	0.7	GD153	5326.2
2	iaai02riq	UVIS1-C512B-SUB (AMP B)	0.8	GD153	6012.3
2	iaai02rjq	UVIS1-C512B-SUB (AMP B)	0.5	GD153	3612.8
2	iaai02rkq	UVIS1-C512B-SUB (AMP B)	30	GD153	229007
2	iaai02rlq	UVIS1-C512B-SUB (AMP B)	1	GD153	7715.4
2	iaai02rmq	UVIS1-C512B-SUB (AMP B)	0.7	GD153	5256.4
2	iaai02rnq	UVIS1-C512B-SUB (AMP B)	0.8	GD153	5984.4
2	iaai02roq	UVIS1-C512B-SUB (AMP B)	0.5	GD153	3618.5
3	iaai03rzq	UVIS2-C512C-SUB (AMP C)	0.5	GD153	3800.9
3	iaai03s0q	UVIS2-C512C-SUB (AMP C)	0.5	GD153	3753.5
3	iaai03s1q	UVIS2-C512C-SUB (AMP C)	0.7	GD153	5521.0
3	iaai03s2q	UVIS2-C512C-SUB (AMP C)	0.7	GD153	5525.6
3	iaai03s3q	UVIS2-C512C-SUB (AMP C)	0.8	GD153	6200.7
3	iaai03s4q	UVIS2-C512C-SUB (AMP C)	0.8	GD153	6327.6
3	iaai03s5q	UVIS2-C512C-SUB (AMP C)	1	GD153	7696.3
3	iaai03s6q	UVIS2-C512C-SUB (AMP C)	30	GD153	234035
3	iaai03s7q	UVIS2-C512C-SUB (AMP C)	0.7	GD153	5316.4
3	iaai03s8q	UVIS2-C512C-SUB (AMP C)	0.8	GD153	6068.6

3	iaai03s9q	UVIS2-C512C-SUB (AMP C)	0.7	GD153	5423.5
3	iaai03saq	UVIS2-C512C-SUB (AMP C)	0.8	GD153	6051.5
3	iaai03sbq	UVIS2-C512C-SUB (AMP C)	0.5	GD153	3716.8
3	iaai03scq	UVIS2-C512C-SUB (AMP C)	0.5	GD153	3912.1
3	iaai03sdq	UVIS2-C512C-SUB (AMP C)	30	GD153	232769
3	iaai03seq	UVIS2-C512C-SUB (AMP C)	1	GD153	7773.8
3	iaai03sfq	UVIS2-C512C-SUB (AMP C)	0.5	GD153	3796.7
3	iaai03sgq	UVIS2-C512C-SUB (AMP C)	0.5	GD153	3675.6
3	iaai03shq	UVIS2-C512C-SUB (AMP C)	0.7	GD153	5543.4
3	iaai03siq	UVIS2-C512C-SUB (AMP C)	0.7	GD153	5269.5
3	iaai03sjq	UVIS2-C512C-SUB (AMP C)	0.8	GD153	6266.4
3	iaai03skq	UVIS2-C512C-SUB (AMP C)	0.8	GD153	6314.6
3	iaai03slq	UVIS2-C512C-SUB (AMP C)	1	GD153	7888.6
3	iaai03smq	UVIS2-C512C-SUB (AMP C)	30	GD153	233381
3	iaai03snq	UVIS2-C512C-SUB (AMP C)	0.7	GD153	5324.7
3	iaai03soq	UVIS2-C512C-SUB (AMP C)	0.8	GD153	6239.7
3	iaai03spq	UVIS2-C512C-SUB (AMP C)	0.7	GD153	5252.8
3	iaai03sqq	UVIS2-C512C-SUB (AMP C)	0.8	GD153	6477.4
3	iaai03srq	UVIS2-C512C-SUB (AMP C)	0.5	GD153	3620.2
3	iaai03ssq	UVIS2-C512C-SUB (AMP C)	0.5	GD153	3701.0
3	iaai03stq	UVIS2-C512C-SUB (AMP C)	30	GD153	234466
3	iaai03suq	UVIS2-C512C-SUB (AMP C)	1	GD153	7664.8
3	iaai03svq	UVIS2-C512C-SUB (AMP C)	0.7	GD153	5484.2
3	iaai03swq	UVIS2-C512C-SUB (AMP C)	0.8	GD153	6203.2
3	iaai03sxq	UVIS2-C512C-SUB (AMP C)	0.5	GD153	3657.0
3	iaai03syq	UVIS2-C512C-SUB (AMP C)	30	GD153	237688
3	iaai03szq	UVIS2-C512C-SUB (AMP C)	1	GD153	7589.3
3	iaai03t0q	UVIS2-C512C-SUB (AMP C)	0.7	GD153	5449.8
3	iaai03t1q	UVIS2-C512C-SUB (AMP C)	0.8	GD153	6178.1
3	iaai03t2q	UVIS2-C512C-SUB (AMP C)	0.5	GD153	3758.8
3	iaai03t3q	UVIS2-C512C-SUB (AMP C)	30	GD153	234155
3	iaai03t4q	UVIS2-C512C-SUB (AMP C)	1	GD153	7773.1
3	iaai03t5q	UVIS2-C512C-SUB (AMP C)	0.7	GD153	5328.2
3	iaai03t6q	UVIS2-C512C-SUB (AMP C)	0.8	GD153	6247.2
3	iaai03t7q	UVIS2-C512C-SUB (AMP C)	0.5	GD153	3872.3

File Type	Header Keyword	Filename	Pedigree
Bad Pixel Table	BPIXTAB	t2c1533si_bpx.fits	TV3
Detector Characteristics Parameters	CCDTAB	t291659mi_ccd.fits	TV3
Detector Overscan Table	OSCTAB	q911321oi_osc.fits	Ground
Bias Image	BIASFILE	b09061275_bia.fits	SMOV
Dark Current Image	DARKFILE	s9j15532i_drk.fits	TV3
Flat Field	PFLTFILE	t4t1832di_pfl.fits	TV3
Multidrizzle Parameter Table	MDRIZTAB	sau1931ai_mdz.fits	TV3

Table 7: Reference files used for the initial CALWF3 processing of the shutter shading data. All files were produced from ground test data except for the bias image, which was derived from earlier SMOV data.

Keyword	Value	Description
GAIN	1.5	CCD gain (e-/DN)
READN	3.	Readnoise (e-)
STATSEC	"*,*"	Section to use for automatic computation of gain
SKYVAL	0.	Sky level that has been subtracted (DN)
SIGCLIP	5.5	Detection limit for cosmic rays (sigma)
SIGFRAC	0.3	Fractional detection limit for neighboring pixels
OBJLIM	2.	Contrast limit between CR and underlying object
NITER	4	Maximum number of iterations
VERBOSE	"yes"	
MODE	"al"	

Table 8: List of parameters used in the IRAF task L.A. Cosmic (van Dokkum 2001) for the removal of cosmic rays.